C.P. No. 245
(17,694)
A.R.C. Technical Report

C.P. No. 245
(17,694)
A.R.C. Technical Report

MINISTRY OF SUPPLY

AERONAUTICAL RESEARCH COUNCIL

CURRENT PAPERS

The Theoretical Wave Drag of Open-Nose Axisymmetrical Forebodies with Varying Fineness Ratio, Area Ratio and Nose Angle

By

J. H. Willis and D. G. Randall, B.Sc.

LONDON: HER MAJESTY'S STATIONERY OFFICE

1956

FIVE SHILLINGS NET

C.P. NO. 245

U.D.C. No. 533.691.18.011.5: 533.6.013.12

Technical Note No. Aero 2360
February, 1955

ROYAL AIRCRAFT ESTABLISHMENT

The Theoretical Wave Drag of Open-nose Axisymmetrical Forebodies with Varying Fineness Ratio, Area Ratio and Nose Angle

by

J.H. Willis*

and

D.G. Randall B.Sc.

SUMMARY

Existing results for the wave drag of open-nose axisymmetrical forebodies are for bodies whose profiles are straight lines or parabolic arcs. These results are here extended to a family of profiles which includes the straight line and the parabolic arc as special cases. Slender body theory is employed throughout.

---

* This work was done while Mr. Willis was on a vacation course at the R.A.E. during July and August, 1954.

LIST OF CONTENTS

LIST OF APPENDICES

LIST OF ILLUSTRATIONS

1 Introduction

Fraenkel[1] has produced results giving the wave drag of open-nose axisymmetrical forebodies* whose profiles are straight lines or parabolic arcs, the latter profiles having zero slope at the position of maximum cross-section. The drags were obtained by use of the two forms of linearised theory, known as slender body theory and quasi-cylinder theory, described in two papers by Lighthill[2,3]. Fraenkel's results have been applied at times to bodies of revolution whose profiles are neither straight lines nor parabolic arcs. In such a case the value obtained for the wave drag is only a crude estimate of its true value. Recently, however, more accurate values of the wave drag have been required. It was decided, therefore, to extend Fraenkel's work so as to include other profile shapes. In this paper a family of profiles which includes the straight line and parabolic arc as special cases will be considered.

Both classes of profiles in Fraenkel's paper depended on two parameters. One of these was taken to be the area ratio, (the ratio of the cross-sectional area at the nose to the maximum cross-sectional area); the other was the fineness ratio, (the ratio of length to maximum radius). The extension to a larger family of profiles introduces a third parameter; this parameter is intimately connected with the slope of the profile at the nose (see equation (1) below). The effect of varying this parameter is shown in Figs. 1(a) and 1(b).

In this paper slender body theory is used throughout. Quasi-cylinder theory applies when the area ratio is close to unity. Fraenkel found that, in this region, the application of slender body theory gave results in good agreement with quasi-cylinder theory. In the region where slender body theory applies i.e. where the fineness ratio is large, the application of quasi-cylinder theory gave results which, in general, differed appreciably from those of slender body theory. Hence, it was decided to dispense with quasi-cylinder theory here and to calculate the wave drags using slender body theory alone.

In view of the reversibility theorem of Ref. 1, the principal drags of the corresponding afterbodies, (obtained by reversing the forebodies), will be the same as the drags of these forebodies.

2 Derivation of Formulae for Drag

The forebodies are assumed to be in a supersonic free-stream of Mach number M, the direction of the free-stream velocity being parallel to the axis of the bodies. The nose of a body is assumed to be $x = 0$ and the maximum cross-section at $x = \ell$, x being measured along the axis. R_o is written for the radius of the body at $x = 0$, and R_m for the maximum radius (occurring at $x = \ell$). S_o is written for the cross-sectional area at $x = 0$, and S_m for the cross-sectional area at $x = \ell$. The profile is assumed to have zero slope at the maximum cross-section, the straight line profile being the only exception to this. $R(x)$ is the value of the radius at station x.

The family of profiles considered has the following equation;

$$R = R_m - (R_m - R_o)\left(1 - \frac{x}{\ell}\right)^n, \quad (n \geq 1). \qquad (1)$$

* Throughout this work it is assumed that the pre-entry stream-tube whose boundary separates the internal and external flows, is cylindrical.

The following substitutions are now made:

$$x/\ell = \xi \tag{2a}$$

$$R/\ell = \theta \tag{2b}$$

$$R_m/\ell = \tau \tag{2c}$$

$$R_o/R_m = \sigma \tag{2d}$$

(1) becomes

$$\theta = \tau\{1 - (1 - \sigma)(1 - \xi)^n\} \tag{3}$$

Differentiation of (1) shows that the slope at the nose is $\frac{n(R_m - R_o)}{\ell}$. If η denotes the nose angle, then

$$\tan \eta = n\tau (1 - \sigma) . \tag{4}$$

Examples of the above family of profiles are shown in Figs.1(a) and 1(b).

If $\ell^2 S(\xi)$ is the cross-sectional area at station ξ, the wave drag of a body, according to slender body theory, is given by

$$\frac{D}{\frac{1}{2}\rho U^2 \ell^2} = -\frac{1}{2\pi}\int_0^1\int_0^1 S''(\xi_1)\, S''(\xi_2) \log|\xi_1 - \xi_2|\, d\xi_1\, d\xi_2$$

$$-2n\, \sigma(1 - \sigma)\tau^2 \int_0^1 S''(\xi) \log \xi\, d\xi + 2\pi\, n^2\, \sigma^2(1 - \sigma)^2\, \tau^4 \log \frac{2}{B\sigma\tau} . \tag{5}$$

In this formula, which is true only if $n > 1$, D is the wave drag of the body, ρ and U are the density and velocity respectively of the free-stream and B is written for $\sqrt{M^2-1}$. ξ_1, ξ_2 are variables of integration and dashes denote differentiation with respect to the independent variable. If $n = 1$ the formula to be used is

$$\frac{D}{\frac{1}{2}\rho U^2 \ell^2} = -\frac{1}{2\pi}\int_0^1\int_0^1 S''(\xi_1)\, S''(\xi_2) \log|\xi_1 - \xi_2|\, d\xi_1\, d\xi_2$$

$$- 2\,(1 - \sigma)\sigma\tau^2 \int_0^1 S''(\xi) \log \xi\, d\xi + 2\,(1 - \sigma)\tau^2 \int_0^1 S''(\xi) \log (1 - \xi) d\xi$$

$$+ 2\pi\,(1 - \sigma^2)\tau^4 \left\{\log \frac{2}{B\tau} + \sigma^2 \log \frac{2}{B\sigma\tau}\right\} \tag{6}$$

(5) and (6) can be derived easily from equation (17) of ref.1 From (3),

$$S(\xi) = \pi\tau^2 \{1 - (1-\sigma)(1-\xi)^n\}^2. \tag{7}$$

Introducing C_D, the drag coefficient based on maximum cross-sectional area, where

$$C_D = \frac{D}{\frac{1}{2}\rho U^2 \ell^2 \pi\tau^2},$$

then, if $n > 1$, (5) and (7) give

$$\frac{C_D}{\tau^2} = -2n^2(1-\sigma)^2 \int_0^1\int_0^1 [(n-1)(1-\xi_1)^{n-2}-(2n-1)(1-\sigma)(1-\xi_1)^{2n-2}]$$

$$[(n-1)(1-\xi_2)^{n-2}-(2n-1)(1-\sigma)(1-\xi_2)^{2n-2}] \log|\xi_1-\xi_2|\, d\xi_1\, d\xi_2$$

$$+4n^2\sigma(1-\sigma)^2 \int_0^1 [(n-1)(1-\xi)^{n-2}-(2n-1)(1-\sigma)(1-\xi)^{2n-2}]\log\xi\, d\xi$$

$$+2n^2\sigma^2(1-\sigma)^2 \log\frac{2}{B\sigma\tau}. \tag{8}$$

Replacing $(1-\xi_1)$, $(1-\xi_2)$ and $(1-\xi)$ by other variables, and using integrals listed in the appendix, (8) becomes

$$\frac{C_D}{\tau^2} = 2(1-\sigma)^2 n^2 \left(\alpha_n + \beta_n\sigma + \gamma_n\sigma^2 + \sigma^2\log\frac{2}{B\sigma\tau}\right), \tag{9}$$

where, if n is an integer,

$$\alpha_n = \sum_{r=1}^{n-1}\frac{1}{r} + \frac{1}{2(n-1)} + \sum_{r=1}^{2n-1}\frac{1}{r} + \frac{1}{2(2n-1)}$$

$$-\frac{2}{(3n-2)}\left[1 + (n-1)\sum_{r=1}^{2n-1}\frac{1}{r} + (2n-1)\sum_{r=1}^{n-1}\frac{1}{r}\right], \tag{10a}$$

$$\beta_n = \frac{2}{3n-2}\left[1 + (n-1)\sum_{r=1}^{2n-1}\frac{1}{r} + (2n-1)\sum_{r=1}^{n-1}\frac{1}{r}\right] - \frac{1}{(2n-1)} - 2\sum_{r=1}^{n-1}\frac{1}{r}, \tag{10b}$$

and

$$\gamma_n = \frac{1}{2(2n-1)} - \sum_{r=1}^{2n-1} \frac{1}{r} . \tag{10c}$$

The formula for the wave drag when $n = {}^3/_2$ was also worked out. Using integrals evaluated in the appendix, and applying (8), it may be shown that this formula is of the same form as (9), but the coefficients are given by

$$\alpha_{3/2} = \frac{3}{20} + \frac{6}{5} \log 2, \tag{11a}$$

$$\beta_{3/2} = \frac{1}{10} + \frac{4}{5} \log 2, \tag{11b}$$

$$\gamma_{3/2} = -\frac{5}{4} . \tag{11c}$$

α_n, β_n, and γ_n are plotted against n in Fig.2.

When n = 1 a similar process applied to (6) and (7) yields the following result for the drag coefficient:

$$\frac{C_D}{\tau^2} = 2(1-\sigma)^2 \left\{ -\tfrac{1}{2} + \sigma - \tfrac{1}{2}\sigma^2 + (1+\sigma^2) \log \frac{2}{B\tau} - \sigma^2 \log \sigma \right\} . \tag{12}$$

The difference in form between (9) and (12) arises because of the extra discontinuity in slope of the straight line profile at the position of maximum cross-section.

3 Discussion of Results

The above equations for the drag are of the form

$$\frac{C_D}{\tau^2} = f(\sigma , B\tau , n) . \tag{13a}$$

This equation can be written as

$$\frac{C_D \ell^2}{R_m^{\ 2}} = f\left(\frac{S_o}{S_m} , B \frac{R_m}{\ell} , n \right) \tag{13b}$$

by using (2c) and (2d).

The results obtained are plotted in Figs.3 to 5 using the form of (13b). For n > 1 the curves of Fig.3 all have the same general shape as those for the parabolic profile, (n = 2). The main effect of an increase in n is an increase in the drag, ceteris paribus; for this reason the vertical scale has had to be compressed for the larger values of n. For n = 1 the curves have a different shape. In particular they do not pass through a common point when $S_o/S_m = 0$ as they do for the other values of n. This is due to the presence of the extra discontinuity in slope at the maximum cross-section. The same curves are plotted logarithmically in Fig. 4; these curves should be used for reading off required drags.

The maximum value of BR_m/ℓ for which the wave drags were evaluated decreases as n increases. This is because, for linearised theory to give physically plausible results, the Mach angle μ must be greater than the nose angle. Hence,

$$\tan\mu > n\frac{R_m}{\ell}(1 - \sigma)$$

i.e.

$$\frac{1}{B} > n\frac{R_m}{\ell}(1 - \sigma)$$

or

$$\frac{BR_m}{\ell} < \frac{1}{n(1 - \sigma)}$$

The curves in Figs. 3 and 4 are drawn only for those values of BR_m/ℓ for which this inequality is satisfied. The inequality may be taken as a rough indication of the limit of applicability of the theory.

The minimum value of the right-hand side occurs when $\sigma = 0$; hence

$$\frac{BR_m}{\ell} < \frac{1}{n} \tag{14}$$

This maximum value of $\frac{BR_m}{\ell}$ decreases as n increases.

In Fig. (5a) $\ell^2 C_D/R_m^{\ 2}$ is plotted against n, $(n > 1)$, for $S_o/S_m = 0$, i.e. for bodies with pointed noses; only one curve occurs since from the form of equation (17) of Ref. 1, it follows that the drag of such bodies is independent of Mach number. This is not true if n = 1 since the discontinuity in the slope at the position of maximum cross-section still occurs.

In Figs. (5b) and (5c) $\ell^2 C_D/R_m^{\ 2}$ is plotted against n, for various values of BR_m/ℓ, for two values of S_o/S_m. (S_o/S_m=0.3 and S_o/S_m=0.7). This shows the general effect on the drag of a variation of n, i.e. of a variation of the slope at the nose. All the curves of Fig. 5 have a minimum between n = 1 and n = 2. However if n is very close to 1, the profile has an extremely rapid change of slope near the position of maximum cross-section. The drags of such unrealistic profiles have no physical significance and the curves of Fig. 5 are of no practical use for values of n very close to 1. Nevertheless, a few values of the wave drag for n = $5/4$ were calculated by a similar method to that of section 2 and these serve to indicate the theoretical behaviour of the curves when n approaches 1. The maximum of the curve for $R_m/\ell = 0.2$ in Fig. 5c at n = 5.5 is almost certainly spurious. It appears because (14) does not hold in the region and so linearised theory is tending to break down.

As regards the accuracy of the results obtained in this paper, it can be stated with confidence that the drags for bodies with sufficiently small values of BR_m/ℓ will be correct, on the basis of linearised theory, since slender body theory holds for such bodies. The phenomenon shown in Fraenkel's work, (agreement of slender body theory with quasi-cylinder theory in regions where the latter but not the former would be expected to hold), suggests that, even for comparatively large BR_m/ℓ, the results are probably still quite close to the correct results based on linearised theory. When BR_m/ℓ approaches $^1/n$, however, linearised theory itself breaks down and results in this region should be viewed with caution.

Fig. 4 can be used for a profile which does not exactly correspond to any member of the family considered here but the probable error in the wave drag in so doing is difficult to estimate. It is possible that profile shapes with identical fineness ratios, area ratios and nose slopes may have wave drags differing considerably from one another. If this were the case, a still larger family of profile shapes incorporating at least one more parameter would have to be considered. The calculation of the wave drags of this family would inevitably be tedious. The only statement that can be made with certainty is that the wave drag of a profile not belonging to the family defined by (1) will be estimated with much more accuracy by the use of Fig. 4 than by the use of the two sets of curves in Ref. 1.

List of Symbols

B	$B = \sqrt{M^2 - 1}$
C_D	Drag coefficient, based on maximum cross-sectional area
D	Wave drag of body of revolution
ℓ	Length of body
M	Free-stream Mach number
m, n	Arbitrary indices in integrals evaluated in Appendix I
n	Parameter of family of profiles defined by equation (1)
$R(x)$	Radius of body at x
R_o	Radius of body at $x = 0$
R_m	Maximum radius of body, always occurring at $x = \ell$
$S(x)$	Cross-sectional area of body at x
S_o	Cross-sectional area of body at $x = 0$
S_m	Cross-sectional area of body at position of maximum radius, ($x = \ell$)
t, u	Variables of integration used in the evaluation of integrals in Appendix I

List of Syrbols (Contd)

U	Free-stream velocity
x	Distance along axis of body measured from nose
$\alpha_n, \beta_n, \gamma_n$	See equations (10) and (11)
η	Nose angle
θ	$\theta = R/\ell$
μ	Semi-angle of Mach cone at the nose of the body
ξ	$\xi = x/\ell$
$\xi_1, \xi_2,$	Variable of integration in equation (5)
ρ	Free-stream density
σ	$\sigma = R_o/R_m$
τ	$\tau = R_m/\ell$

Dashes denote differentiation with respect to the independent variable.

References

No.	Author	Title etc.
1	L.E. Fraenkel	The theoretical wave drag of some bodies of revolution. R & M 2842 May, 1951
2	M.J. Lighthill	Supersonic flow past bodies of revolution. R & M 2003, 1945
3	M.J. Lighthill	Supersonic flow past slender bodies of revolution the slope of whose meridion section is discontinuous. Quarterly Journal of Mechanics and Applied Mathematics, Vol. 1, Part 1, March 1948

Appendix I

Evaluation of some Integrals

1.

$$-\int_0^1 x^n \log(1-x)\,dx$$

$$= \int_0^1 \left\{\left(\frac{1}{n+1} - x^n\right)\log(1-x) - \frac{1}{n+1}\log(1+x)\right\}dx$$

$$= \left[\left(\frac{x}{n+1} - \frac{x^{n+1}}{n+1}\right)\log(1-x)\right]_0^1 + \int_0^1 \left(\frac{x}{n+1} - \frac{x^{n+1}}{n+1}\right)\frac{dx}{1-x} + \frac{1}{n+1}\left[(1-x)\log(1-x) - (1-x)\right]_0^1$$

$$= \frac{1}{n+1}\int_0^1 \sum_{r=1}^{n} x^r\,dx + \frac{1}{n+1} = \frac{1}{n+1}\sum_{r=1}^{n+1}\frac{1}{r} \qquad I(1)$$

2.

$$-\int_0^1\int_0^1 x^n y^m \log|x-y|\,dx\,dy$$

Consider

$$-\int_0^1 y^m \log|x-y|\,dy$$

This is the same as

$$-\left[\frac{y^{m+1}}{m+1}\log|x-y|\right]_0^1 + \int_0^1 \frac{y^{m+1}}{m+1}\frac{dy}{y-x}$$

$$= -\frac{\log(1-x)}{m+1} + \frac{1}{m+1}\int_0^1 \frac{y^{m+1}-x^{m+1}}{y-x}\,dy + \frac{x^{m+1}}{m+1}\int_0^1 \frac{dy}{y-x}$$

$$= -\frac{\log(1-x)}{m+1} + \frac{1}{m+1}\int_0^1 \sum_{r=1}^{m+1} x^{r-1}y^{m-r+1}\,dy + \frac{x^{n+1}}{m+1}\left[\log|y-x|\right]_0^1$$

$$= -\frac{\log(1-x)}{m+1} + \frac{1}{m+1}\sum_{r=1}^{m+1}\frac{x^{r-1}}{m-r+2} + \frac{x^{m+1}}{m+1}\log(1-x) - \frac{x^{m+1}}{m+1}\log x$$

$\therefore$ By using I(1), $-\int_0^1\int_0^1 x^n y^m \log|x-y|\,dx\,dy$ may be written as

$$\frac{1}{(m+1)(n+1)}\sum_{r=1}^{n+1}\frac{1}{r}+\frac{1}{(m+1)}\sum_{r=1}^{m+1}\frac{1}{(m-r+2)(n+r)}-\frac{1}{(m+1)(m+n+2)}\sum_{r=1}^{m+n+2}\frac{1}{r}+\frac{1}{(m+1)(m+n+2)^2},$$

$$=\frac{1}{(m+n+2)}\left(\frac{1}{m+1}+\frac{1}{n+1}\right)\sum_{r=1}^{n+1}\frac{1}{r}+\frac{1}{(m+1)(m+n+2)}\sum_{r=1}^{m+1}\left(\frac{1}{m-r+2}+\frac{1}{n+r}\right)-\frac{1}{(n+1)}\left(\frac{1}{m+1}-\frac{1}{m+n+2}\right)\sum_{r=1}^{m+n+1}\frac{1}{r}$$

$$=\frac{1}{(m+n+2)(n+1)}\sum_{r=1}^{n+1}\frac{1}{r}+\frac{1}{(m+n+2)(m+1)}\sum_{r=1}^{m+1}\frac{1}{r}+\frac{1}{(m+1)(n+1)(m+n+2)} \qquad \text{I(2)}$$

Some numerical values of this integral are given in the following table.

TABLE I

Values of the integral $-\int_0^1\int_0^1 x^n y^m \log|x-y|\,dx\,dy$

n \ m	0	1	2	3	4
0	1.5000	0.7500	0.4861	0.3542	0.2761
1	0.7500	0.4375	0.3056	0.2326	0.1867
2	0.4861	0.3056	0.2222	0.1736	0.1418
3	0.3542	0.2326	0.1736	0.1380	0.1142
4	0.2761	0.1867	0.1418	0.1142	0.0953

3. $$-\int_0^1 x^{-\frac{1}{2}}\log(1-x)\,dx$$

Put $x = t^2$. The integral becomes

$$-2\int_0^1 \log(1-t^2)\,dt = -2\int_0^1 \{\log(1-t)+\log(1+t)\}\,dt$$

$$= -2\left[-(1-t)\log(1-t)+(1-t)+(1+t)\log(1+t)-(1+t)\right]_0^1$$

$$= 4(1-\log 2) \qquad \text{I(3)}$$

4.

$$-\int_0^1\int_0^1 x^{-\frac{1}{2}}\, y \log |x-y|\, dx\, dy$$

Put $x = t^2$, $y = u^2$. The integral becomes

$$-4\int_0^1\int_0^1 u^3 \log |t^2-u^2|\, dt\, du$$

$$= -4\int_0^1\int_0^1 u^3 \{\log (t+u)+\log |t-u|\}dt\, du$$

$$= -4\int_0^1 u^3 \left[(t+u)\log (t+u)-(t+u)+(t-u)\log (t-u)-(t-u)\right]_0^1 du$$

$$= -4\int_0^1 u^3 \left[(1+u)\log (1+u)+(1-u)\log (1-u)-2\right]du \qquad I(4)$$

Now

$$\int_0^1 (u^3+u^4)\log (1+u)\, du = \left[\left(\frac{u^4}{4}+\frac{u^5}{5}\right)\log (1+u)\right]_0^1 - \int_0^1 \left(\frac{u^4}{4}+\frac{u^5}{5}\right)\frac{du}{1+u}$$

$$= \frac{9}{20}\log 2 - \frac{1}{20}\int_0^1 \left[4u^4+u^3-u^2+u-1+\frac{1}{u+1}\right]du$$

$$= \frac{9}{20}\log 2-\frac{1}{20}\left[\frac{4}{5}+\frac{1}{4}-\frac{1}{3}+\frac{1}{2}-1+\log 2\right] = \frac{2}{5}\log 2-\frac{13}{1,200} \qquad I(5)$$

Using I(1)

$$-\int_0^1 (u^3-u^4)\log (1-u)\, du = \frac{1}{4}\sum_{r=1}^{4}\frac{1}{r}-\frac{1}{5}\sum_{r=1}^{5} = \frac{77}{1,200} \qquad I(6)$$

$\therefore$ By I(4), I(5) and I(6)

$$-\int_0^1\int_0^1 x^{-\frac{1}{2}}\, y \log |x-y|\, dx\, dy = -\frac{8}{5}\log 2+\frac{13}{300}+\frac{77}{300}+2$$

$$= \frac{23}{10}-\frac{8}{5}\log 2 \qquad I(7)$$

5. $$-\int_0^1\int_0^1 x^{-\frac{1}{2}}\, y^{-\frac{1}{2}} \log|x-y|\, dx\, dy$$

Put $x = t^2$, $y = u^2$. The integral becomes

$$-4\int_0^1\int_0^1 \log|t^2-u^2|\, dt\, du = -4\int_0^1\int_0^1 \{\log(t+u)+\log|t-u|\}\, dt\, du$$

$$= -4\int_0^1 \Big[(t+u)\log(t+u)-(t+u)+(t-u)\log|t-u| - (t-u)\Big]_0^1\, du$$

$$= -4\int_0^1 [(1+u)\log(1+u)+(1-u)\log(1-u) - 2]\, du$$

$$= -4\left[\frac{(1+u^2)}{2}\log(1+u)-\frac{(1+u)^2}{4}-\frac{(1-u)^2}{2}\log(1-u)+\frac{(1-u)^2}{4} - 2u\right]_0^1$$

$$= -4\left[2\log 2 - 1 - 2 + \frac{1}{4}-\frac{1}{4}\right] = 12 - 8\log 2 \qquad \text{I(8)}$$

Wt.2078. CP245.K3 - Printed In Great Britain.

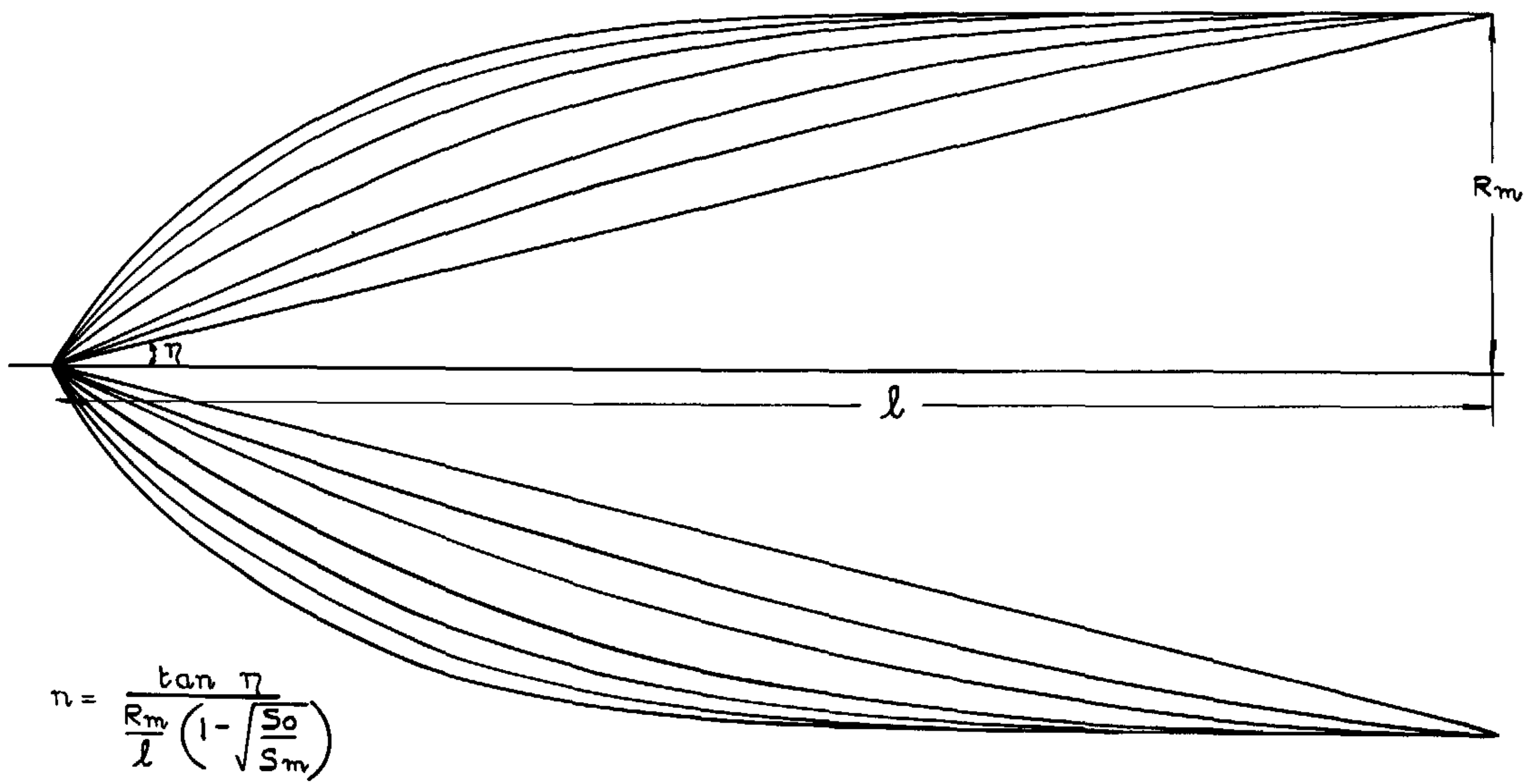

FIG. 1(a). EXAMPLES OF PROFILES FOR $\frac{S_o}{S_m} = 0$, $\frac{R_m}{l} = 0{\cdot}25$ AND $n = 1$ (INNER CURVE), $3/2$, 2, 3, 4, 5, 6, (OUTER CURVE).
I.E. $\tan\eta = 0{\cdot}25$, $0{\cdot}375$, $0{\cdot}50$, $0{\cdot}75$, $1{\cdot}00$, $1{\cdot}25$, $1{\cdot}50$.

FIG. 1(b)

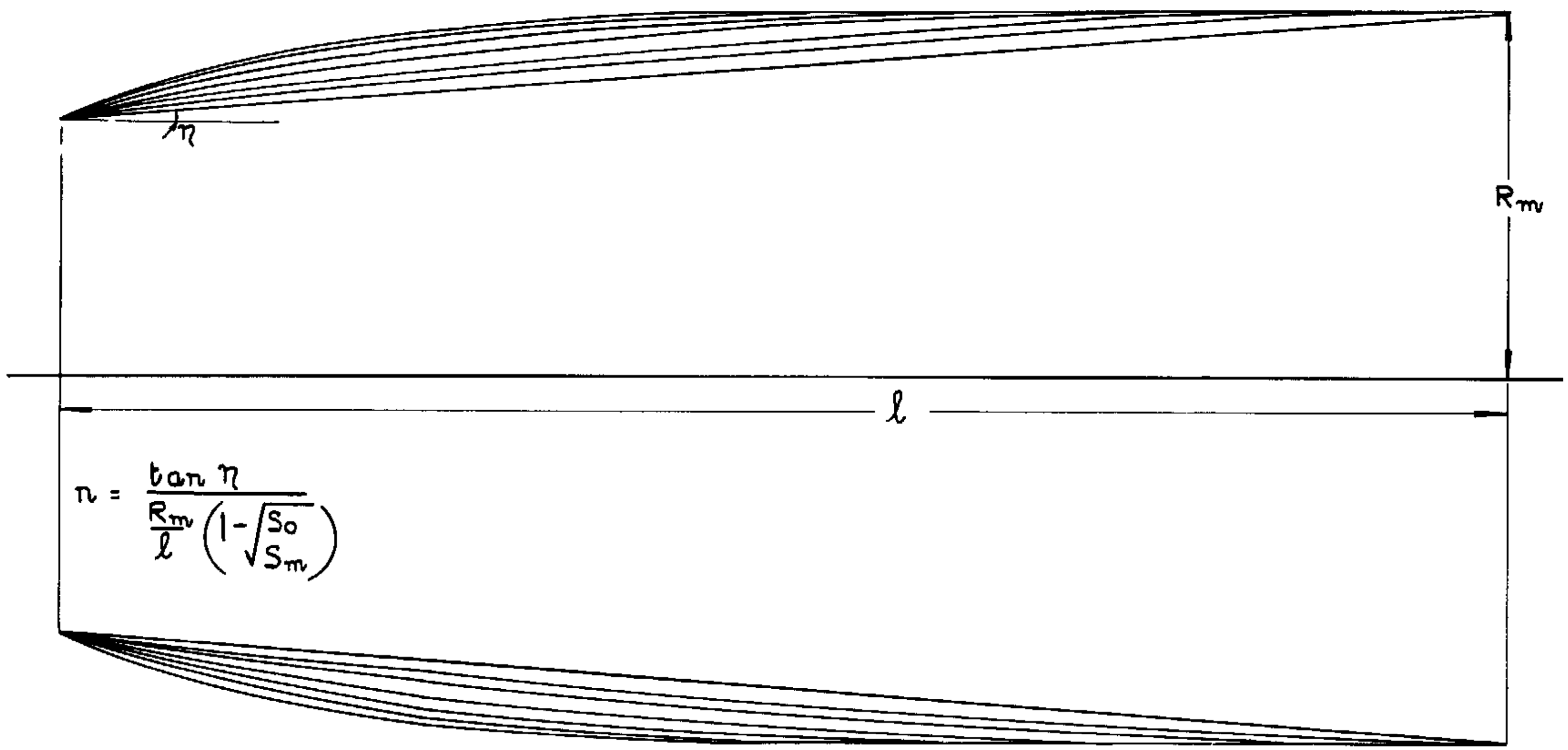

FIG. 1(b) EXAMPLES OF PROFILES FOR $\frac{S_o}{S_m} = 0{\cdot}49$, $\frac{R_m}{\ell} = 0{\cdot}25$, AND $n = 1$ (INNER CURVE), $3/2$, 2, 3, 4, 5, 6, (OUTER CURVE).

I.E. $\eta = 0{\cdot}075$, $0{\cdot}1125$, $0{\cdot}150$, $0{\cdot}225$, $0{\cdot}300$, $0{\cdot}375$, $0{\cdot}450$.

FIG.2

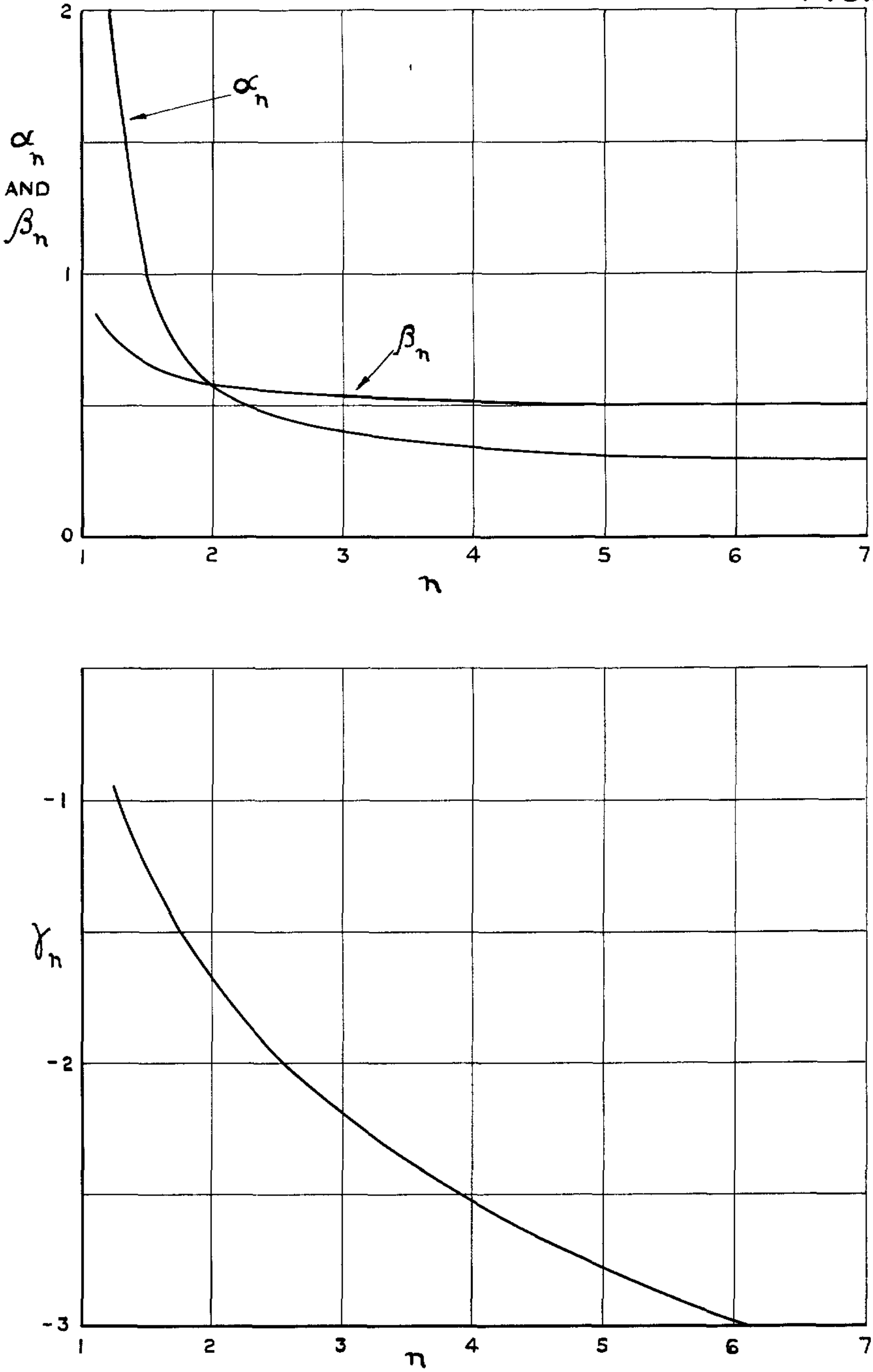

FIG.2 VALUES OF COEFFICIENTS IN DRAG EQUATION, (9), FOR VARYING n

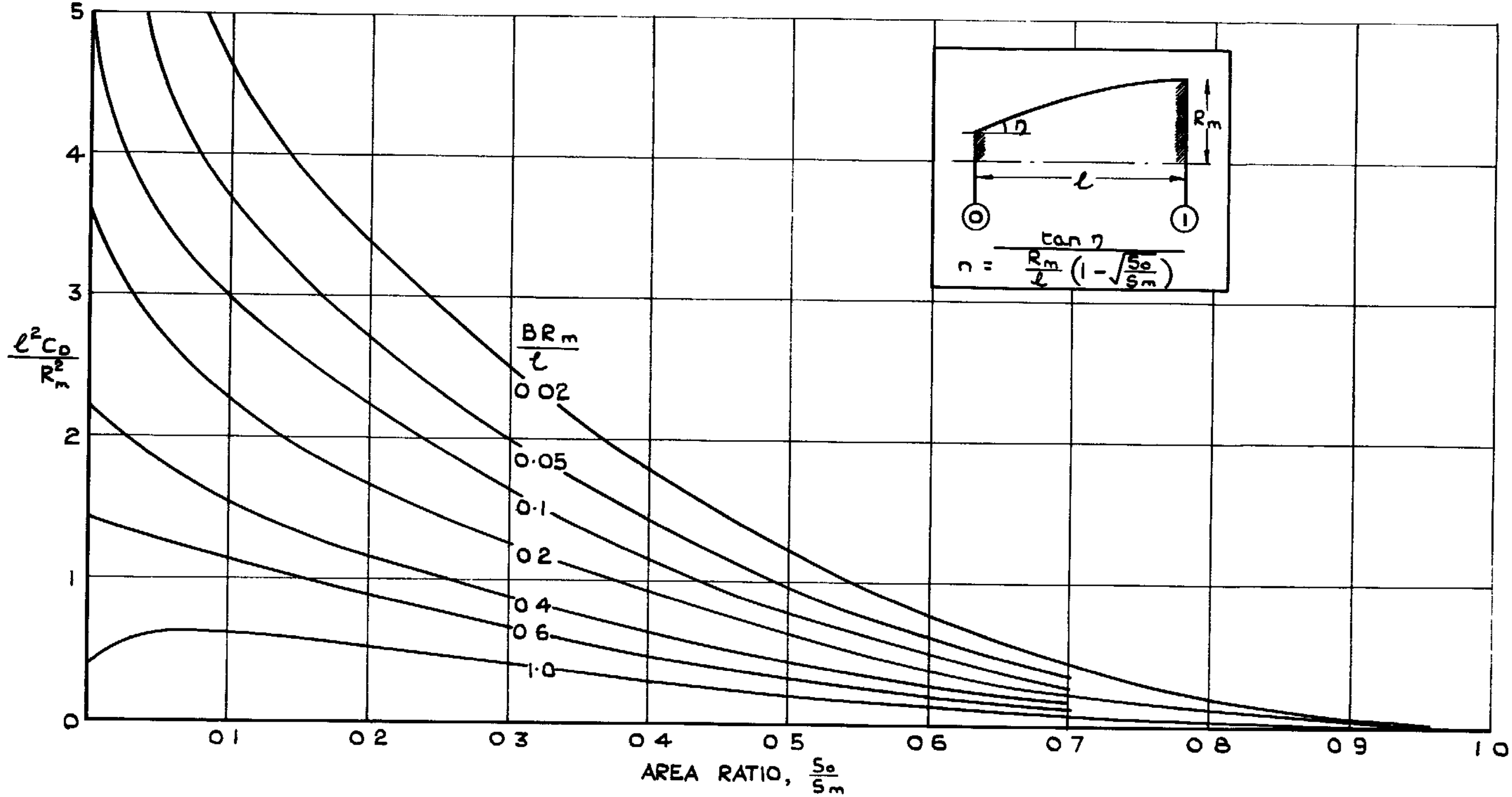

FIG. 3(a) DRAG OF FOREBODIES WITH n=1 (STRAIGHT LINE PROFILE.)

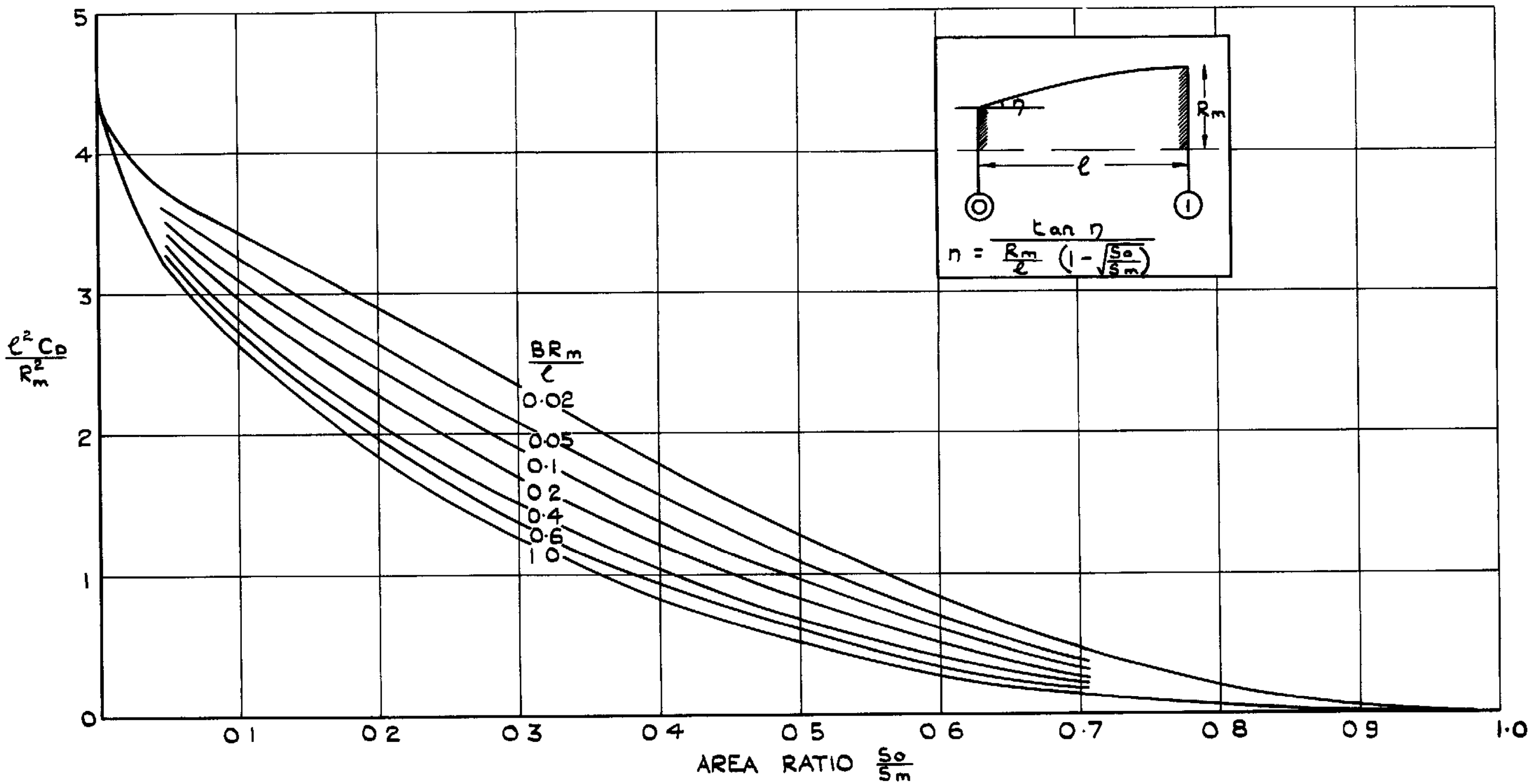

FIG. 3(b) DRAG OF FOREBODIES WITH $n = 3/2$.

FIG. 3(b)

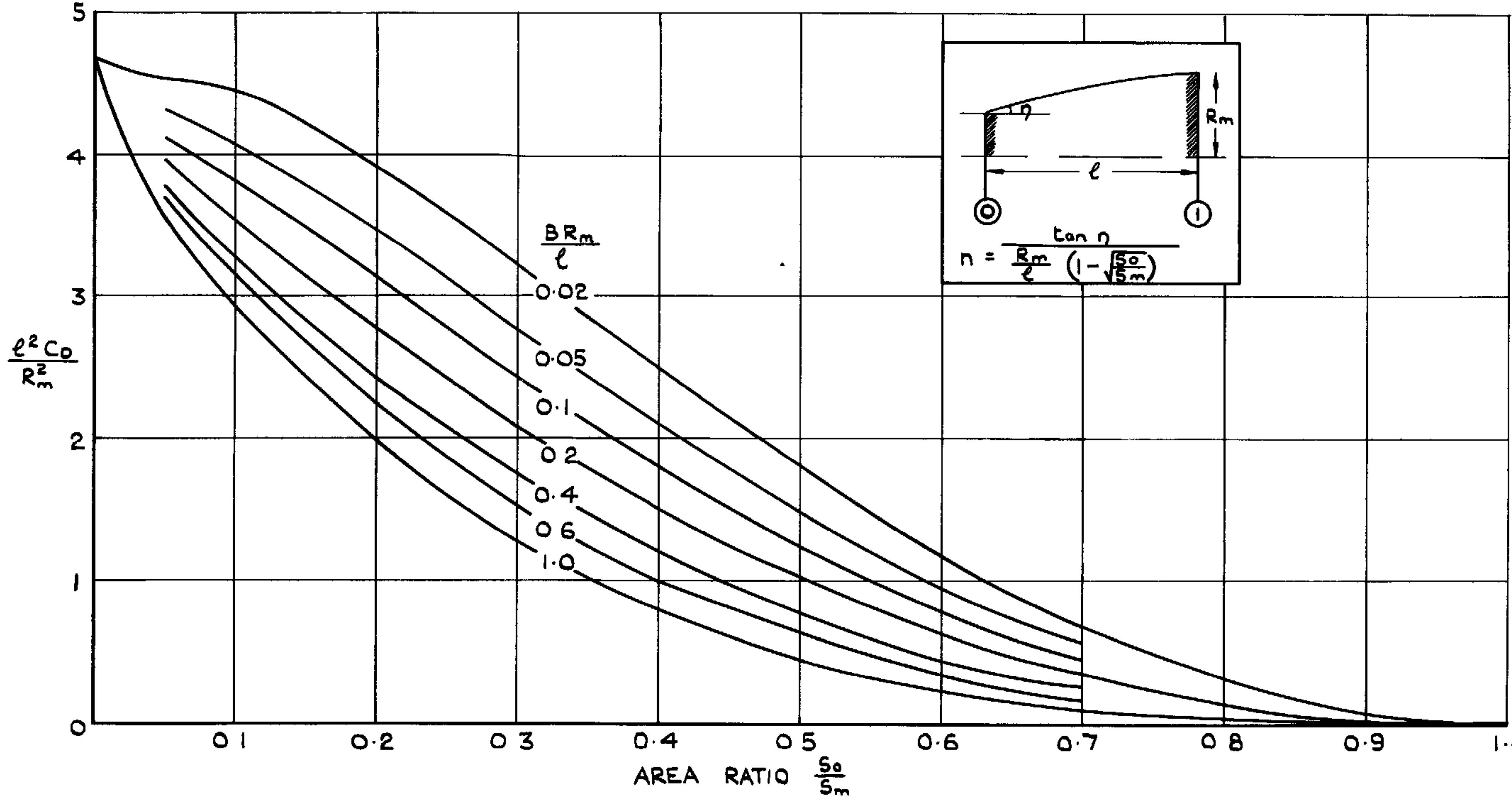

FIG. 3 (c) DRAG OF FOREBODIES WITH n = 2 (PARABOLIC ARC PROFILE.)

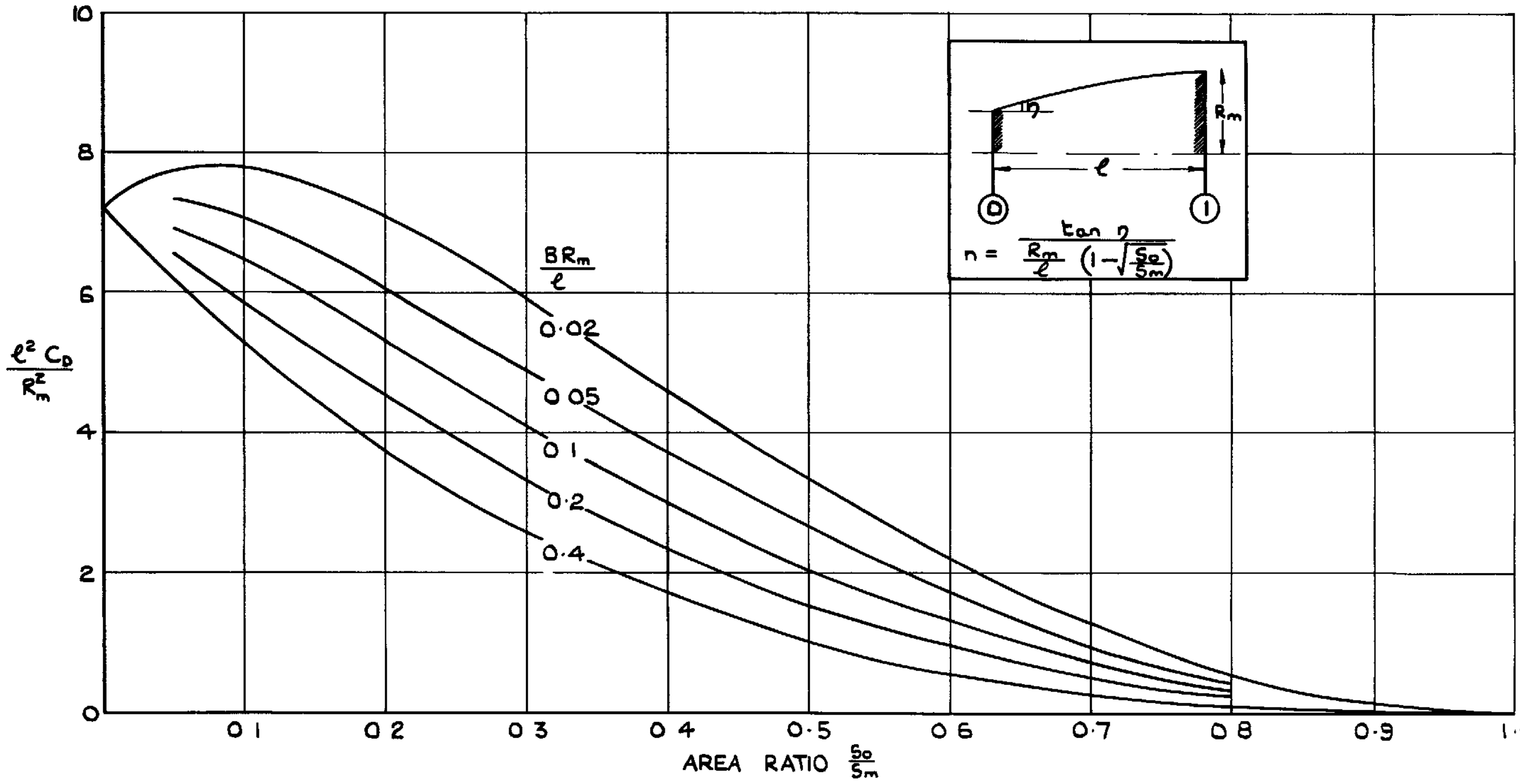

FIG. 3 (d) DRAG OF FOREBODIES WITH n = 3.

FIG. 3 (e)

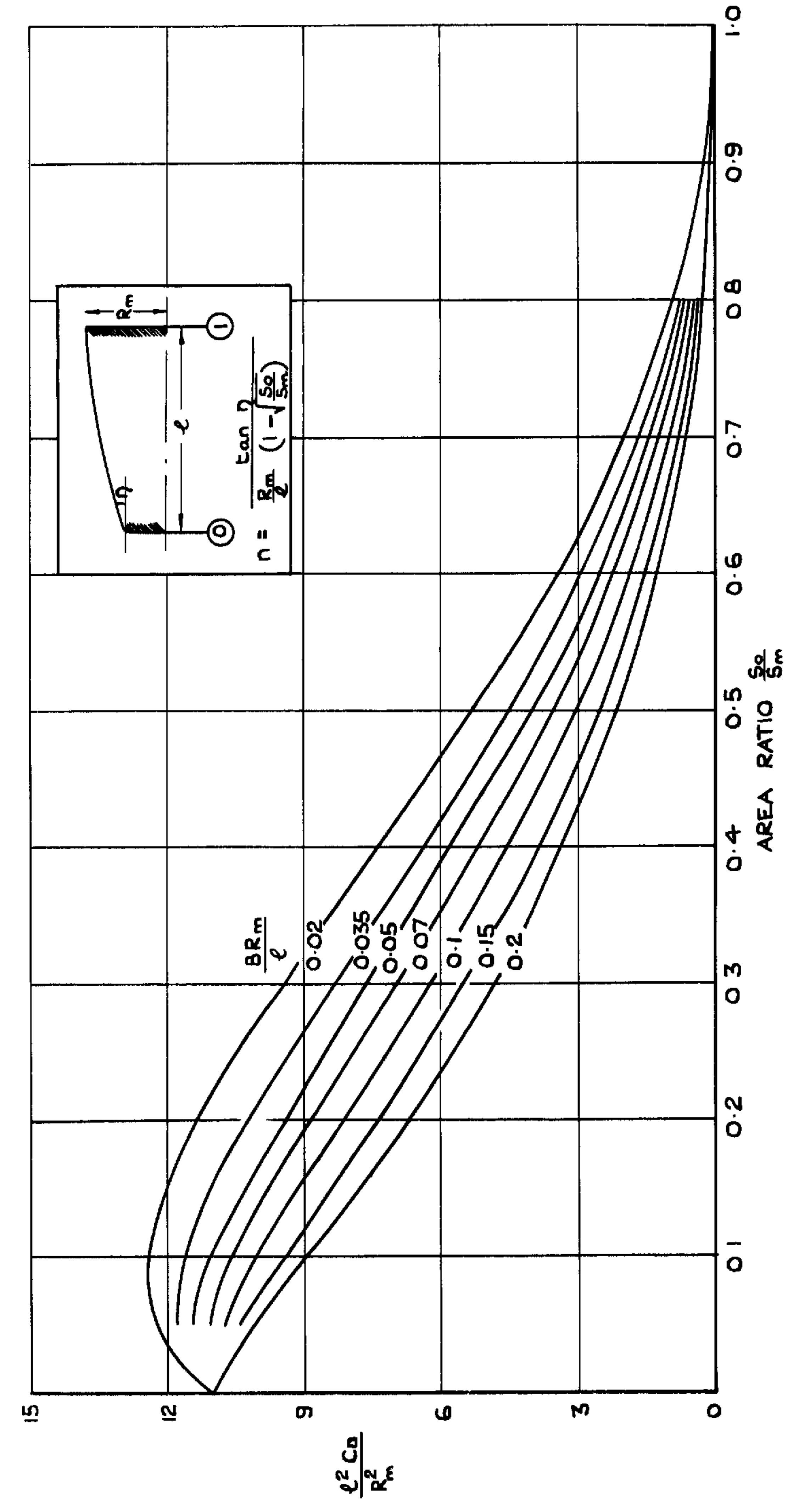

FIG. 3 (e) DRAG OF FOREBODIES WITH n = 4.

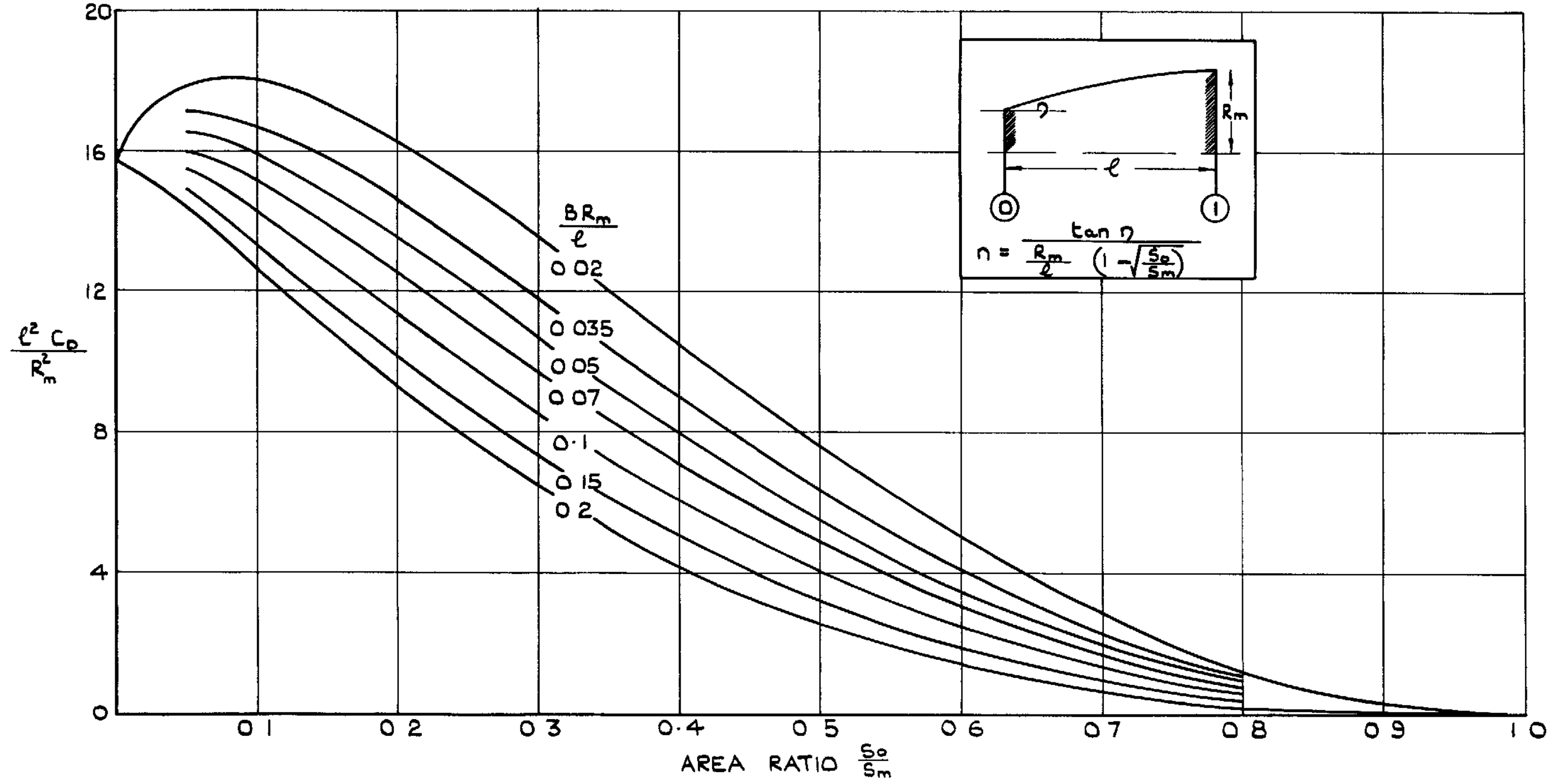

FIG. 3 (f) DRAG OF FOREBODIES WITH n = 5.

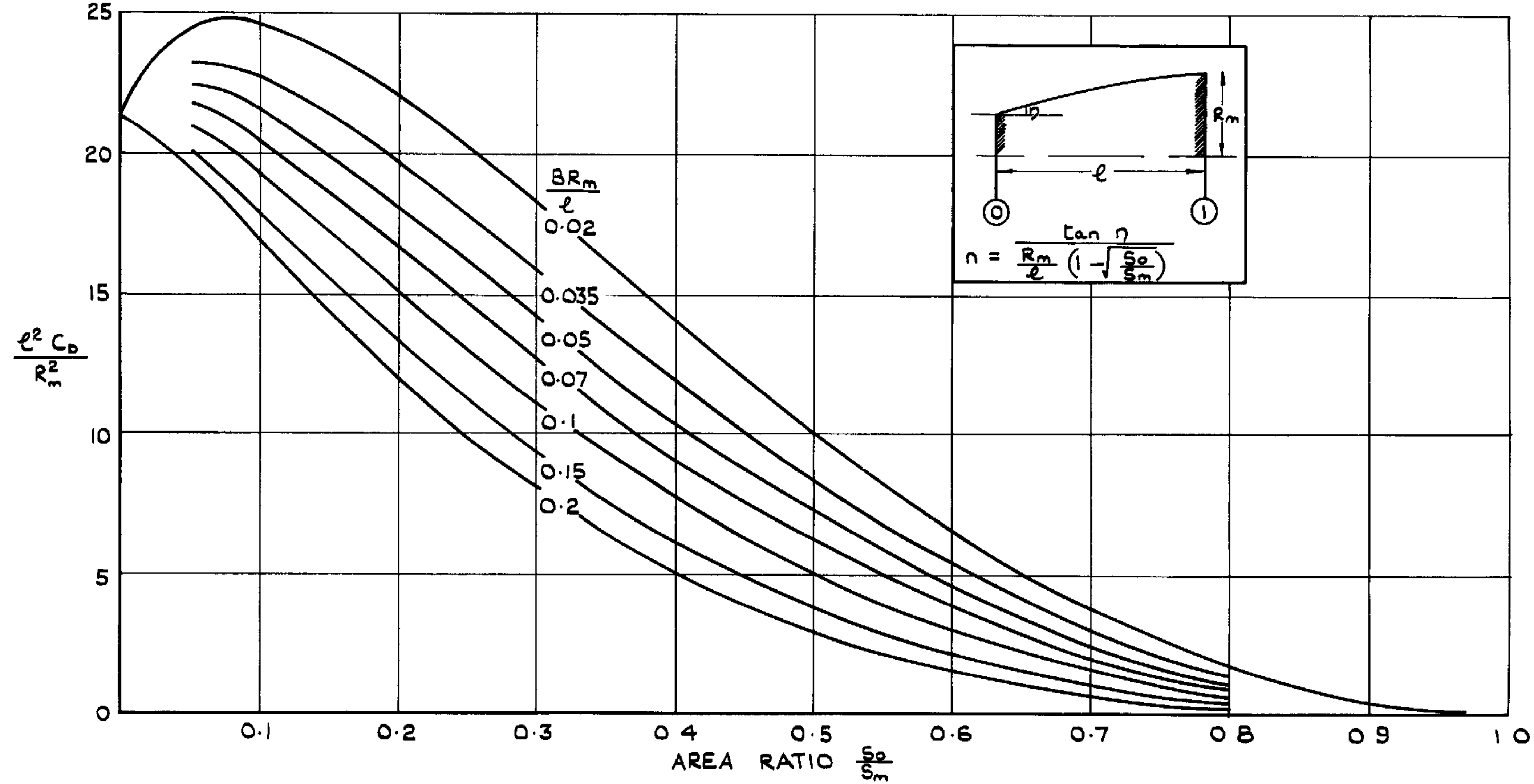

FIG 3(g) DRAG OF FOREBODIES WITH n = 6.

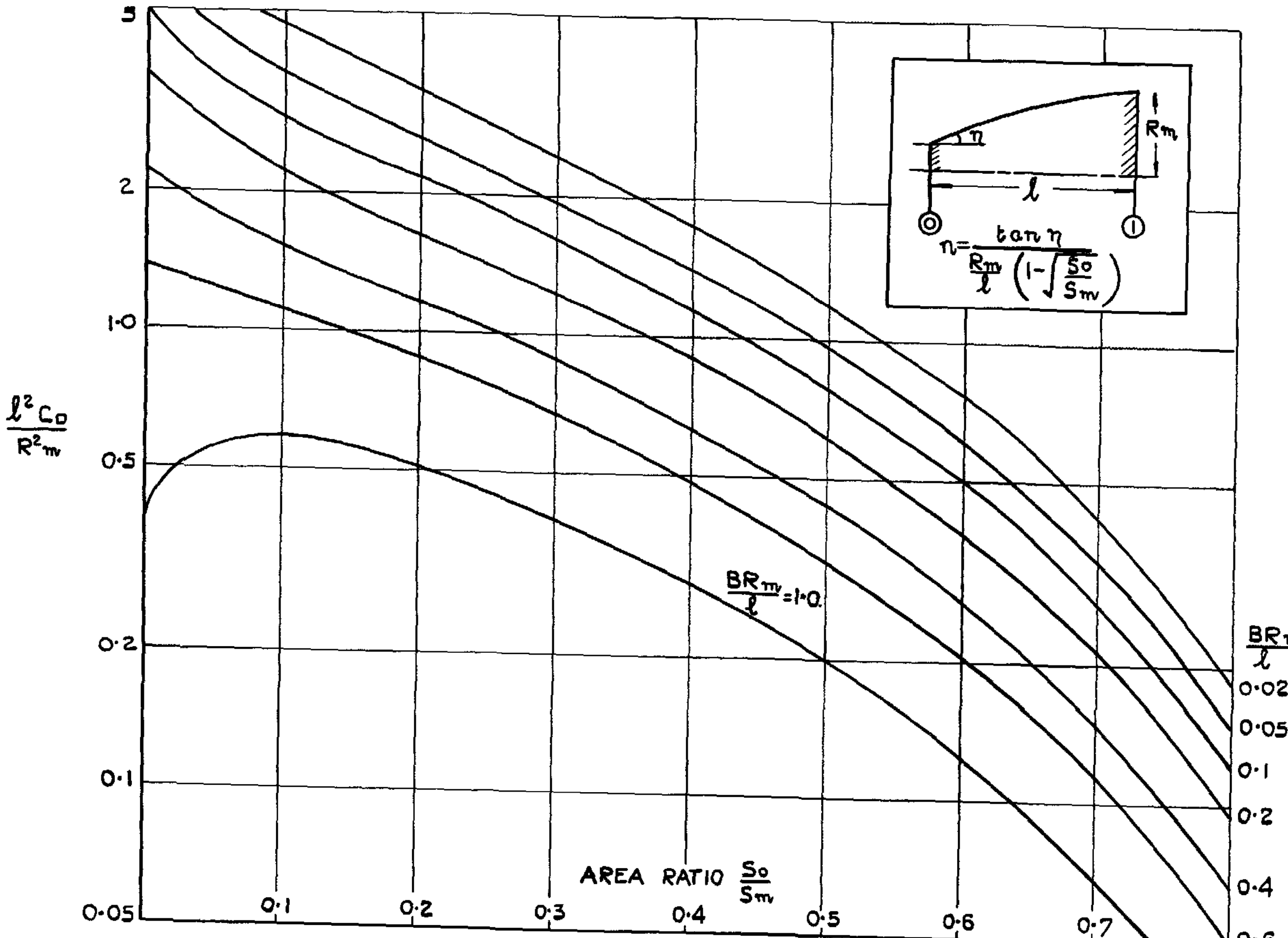

FIG. 4(a). DRAG OF FOREBODIES WITH $n = 1$ (STRAIGHT LINE PROFILE)

FIG. 4(a).

FIG. 4(b).

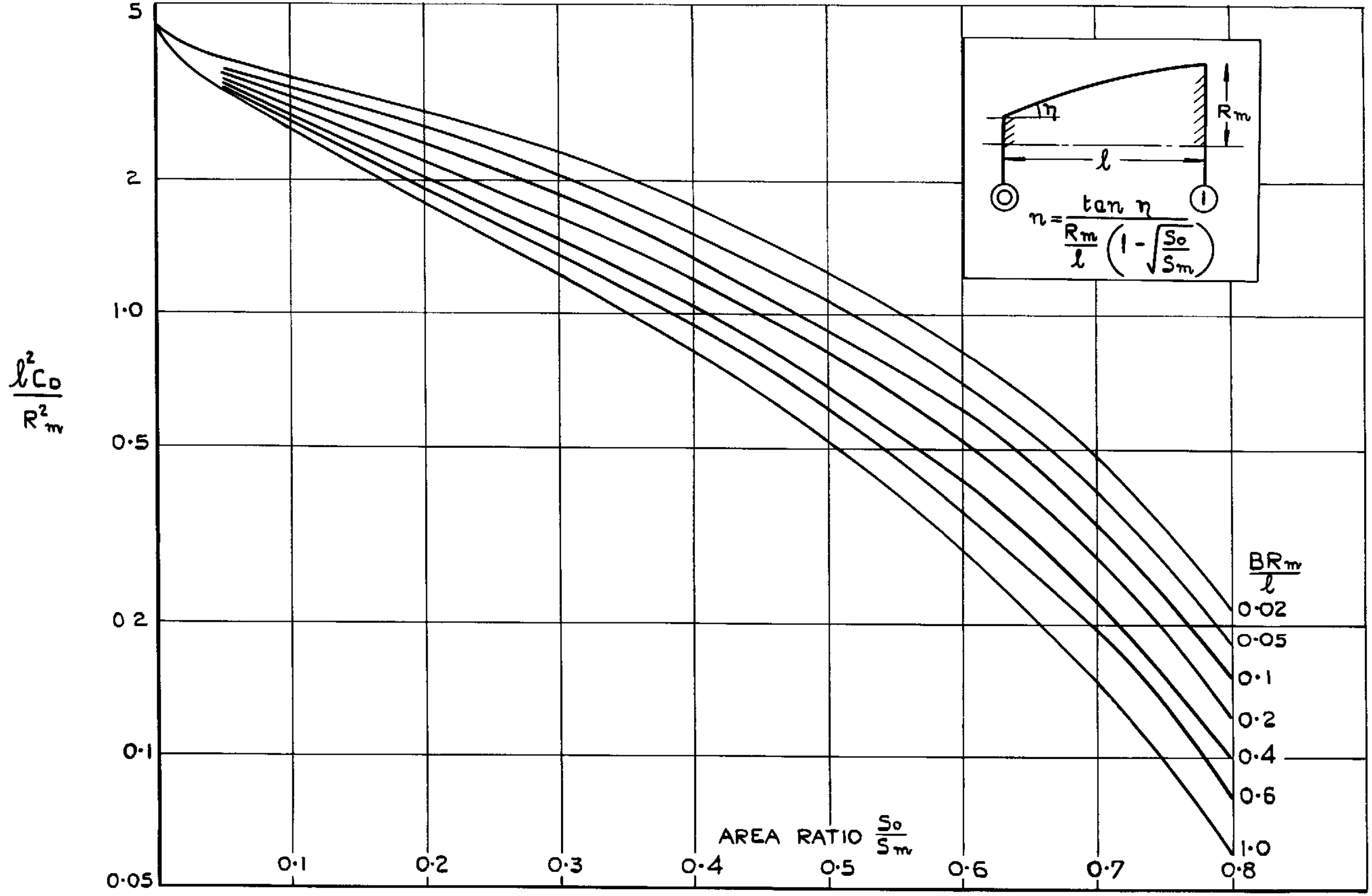

FIG. 4 (b) DRAG OF FOREBODIES WITH $n = 3/2$.

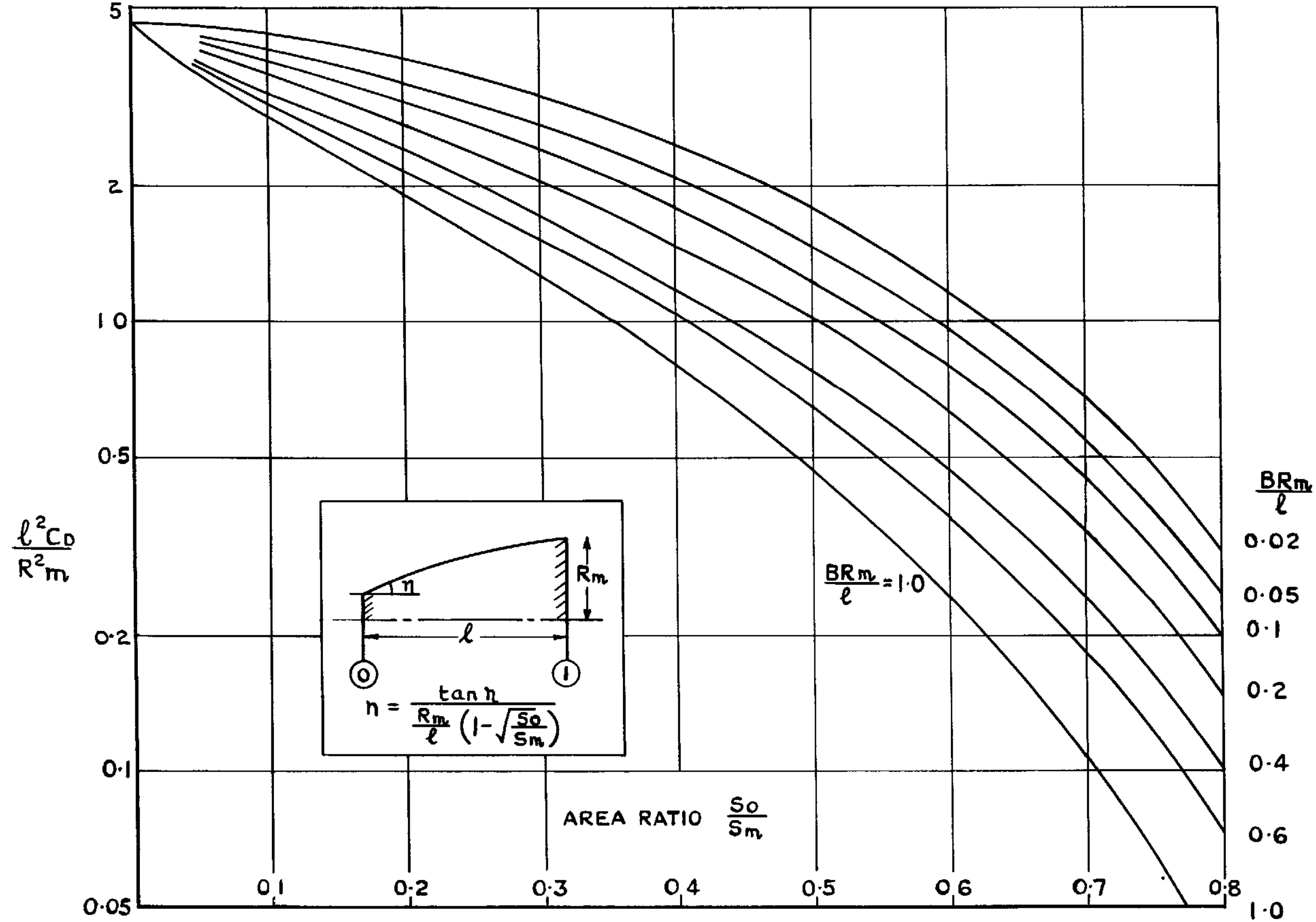

FIG. 4(C) DRAG OF FOREBODIES WITH $n = 2$ (PARABOLIC ARC PROFILE)

FIG. 4(C)

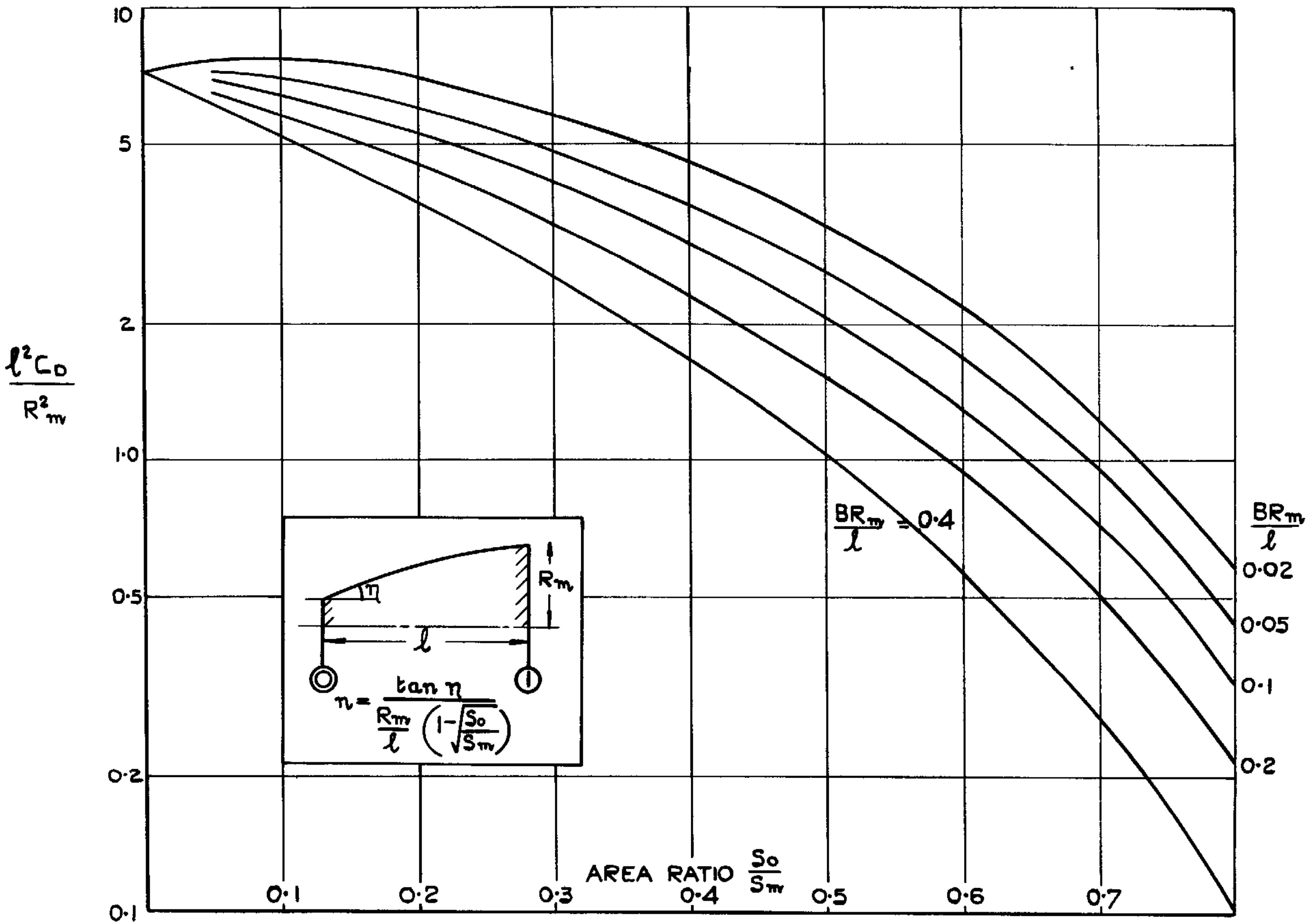

FIG. 4 (d). DRAG FOREBODIES WITH $n = 3$.

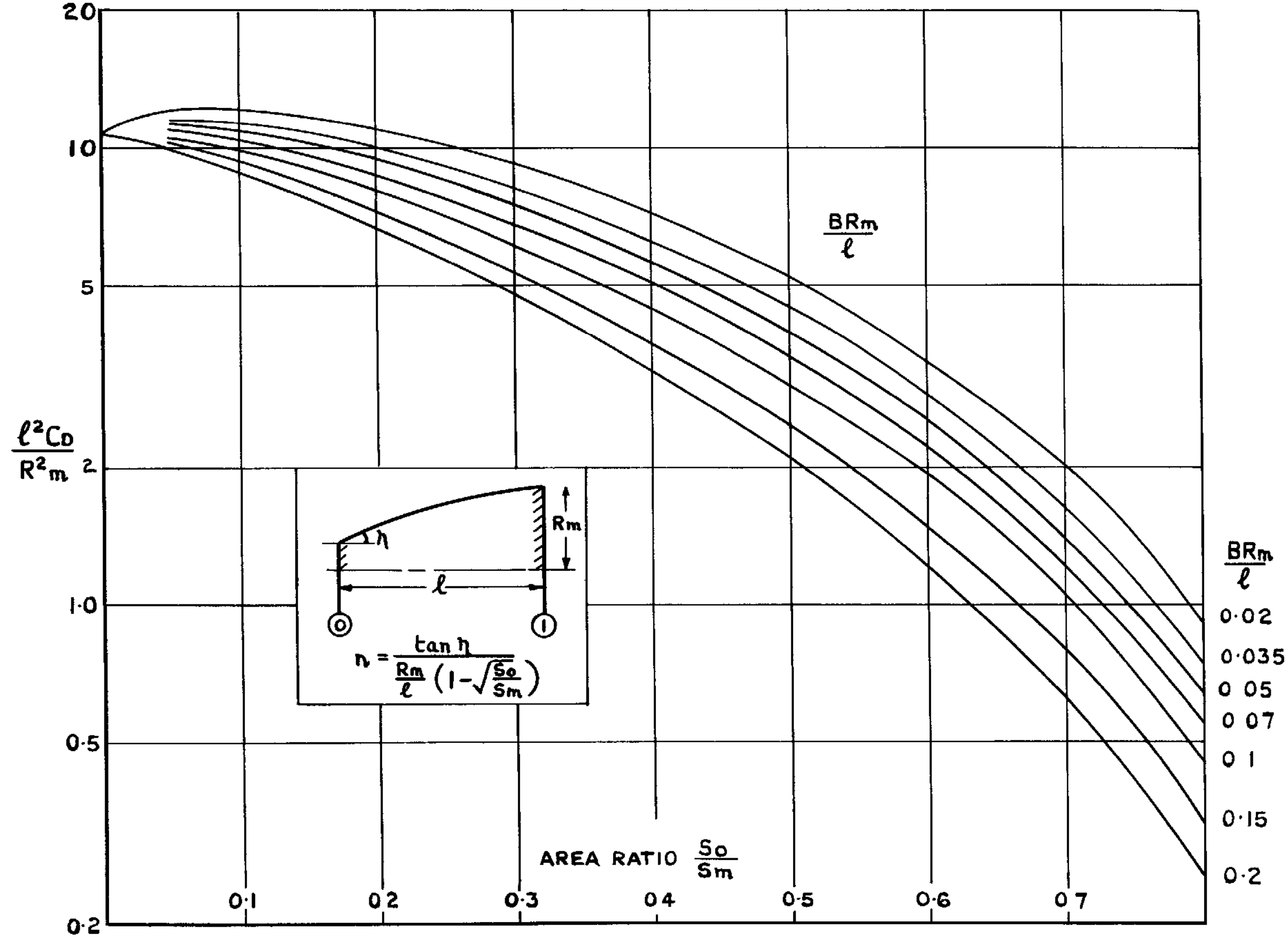

FIG.4 (e) DRAG OF FOREBODIES WITH $n = 4$

FIG.4 (e)

FIG. 4 (f)

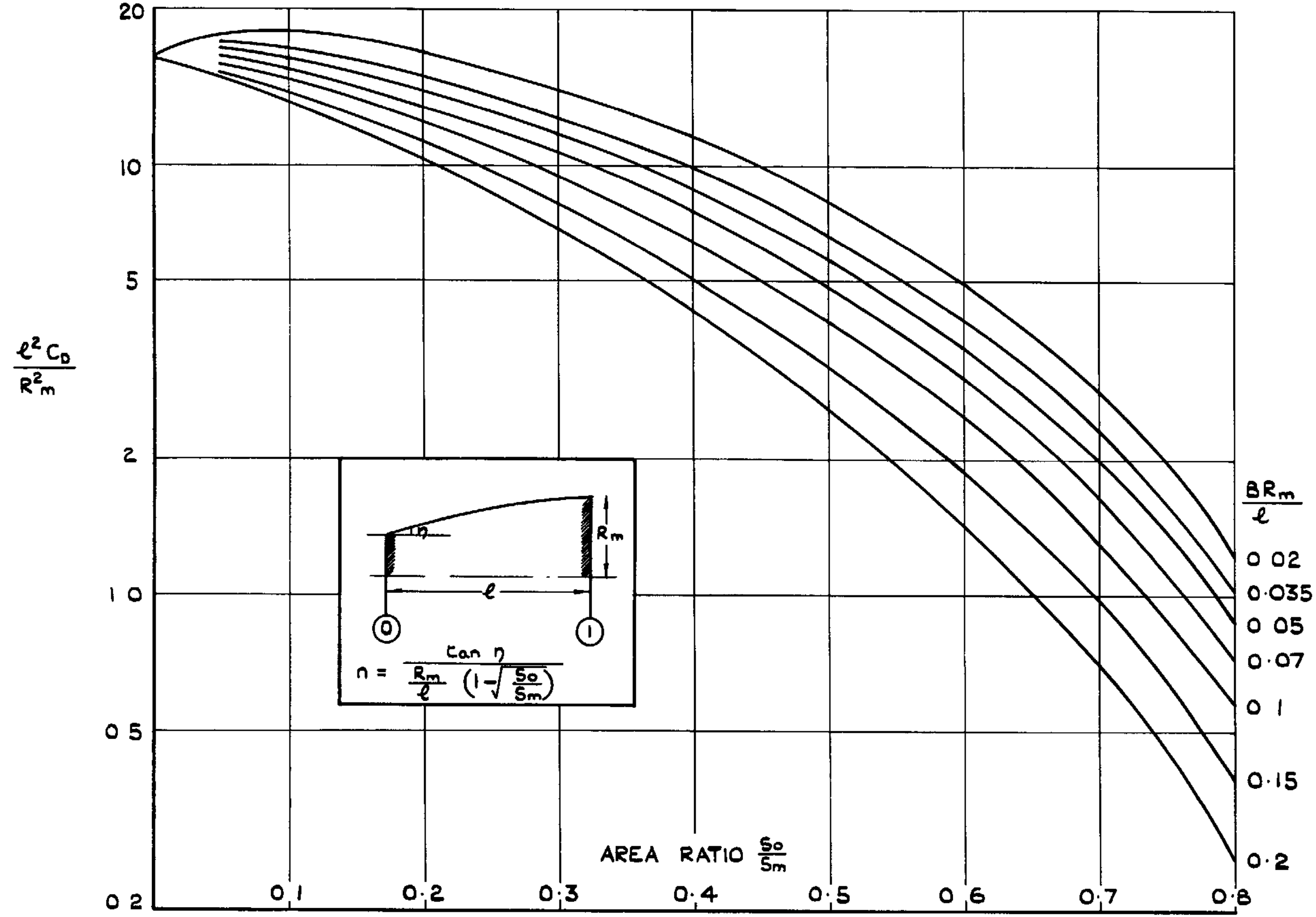

FIG. 4 (f) DRAG OF FOREBODIES WITH n = 5.

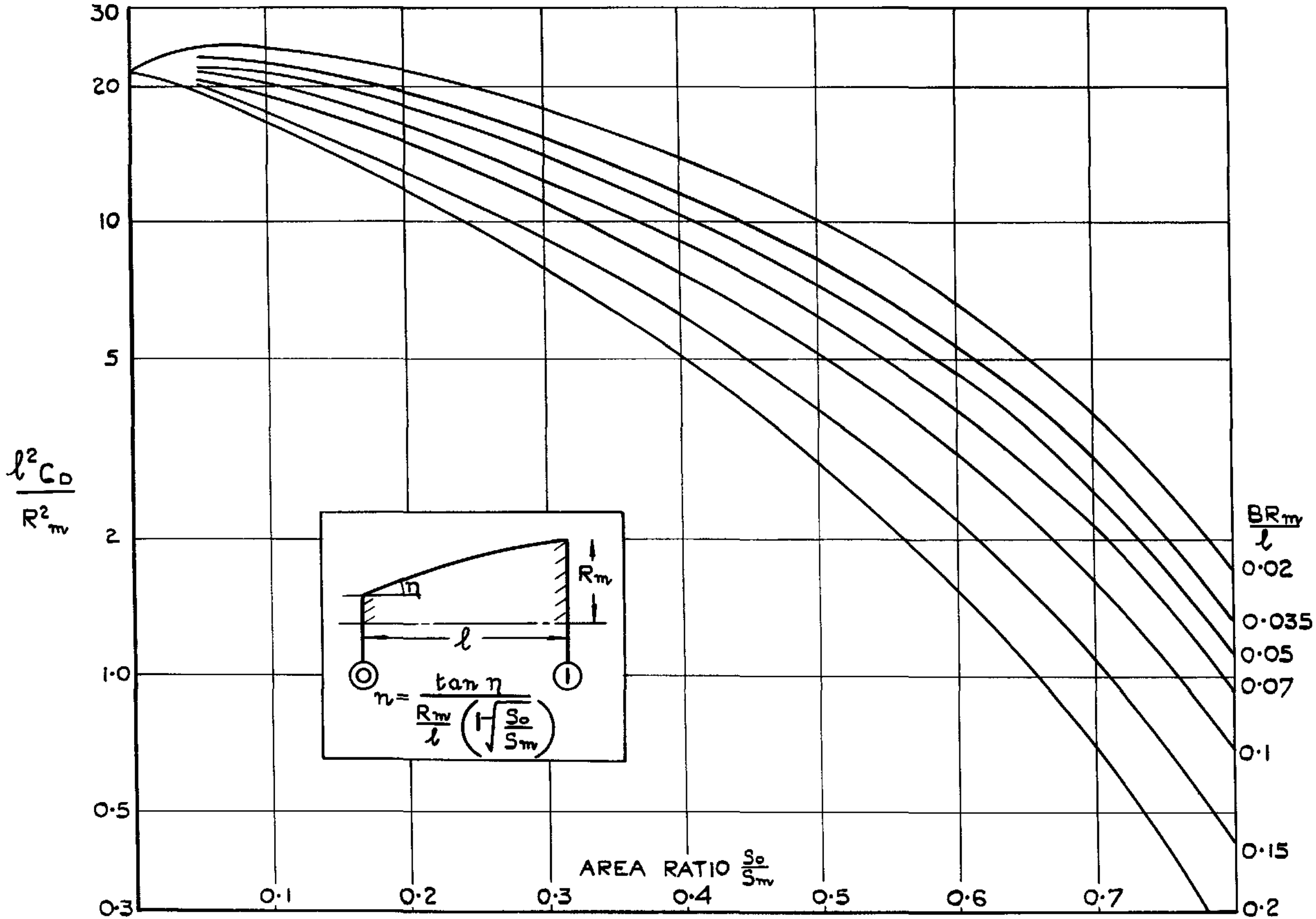

FIG. 4(g). DRAG OF FOREBODIES WITH $n = 6$.

FIG.5(a)

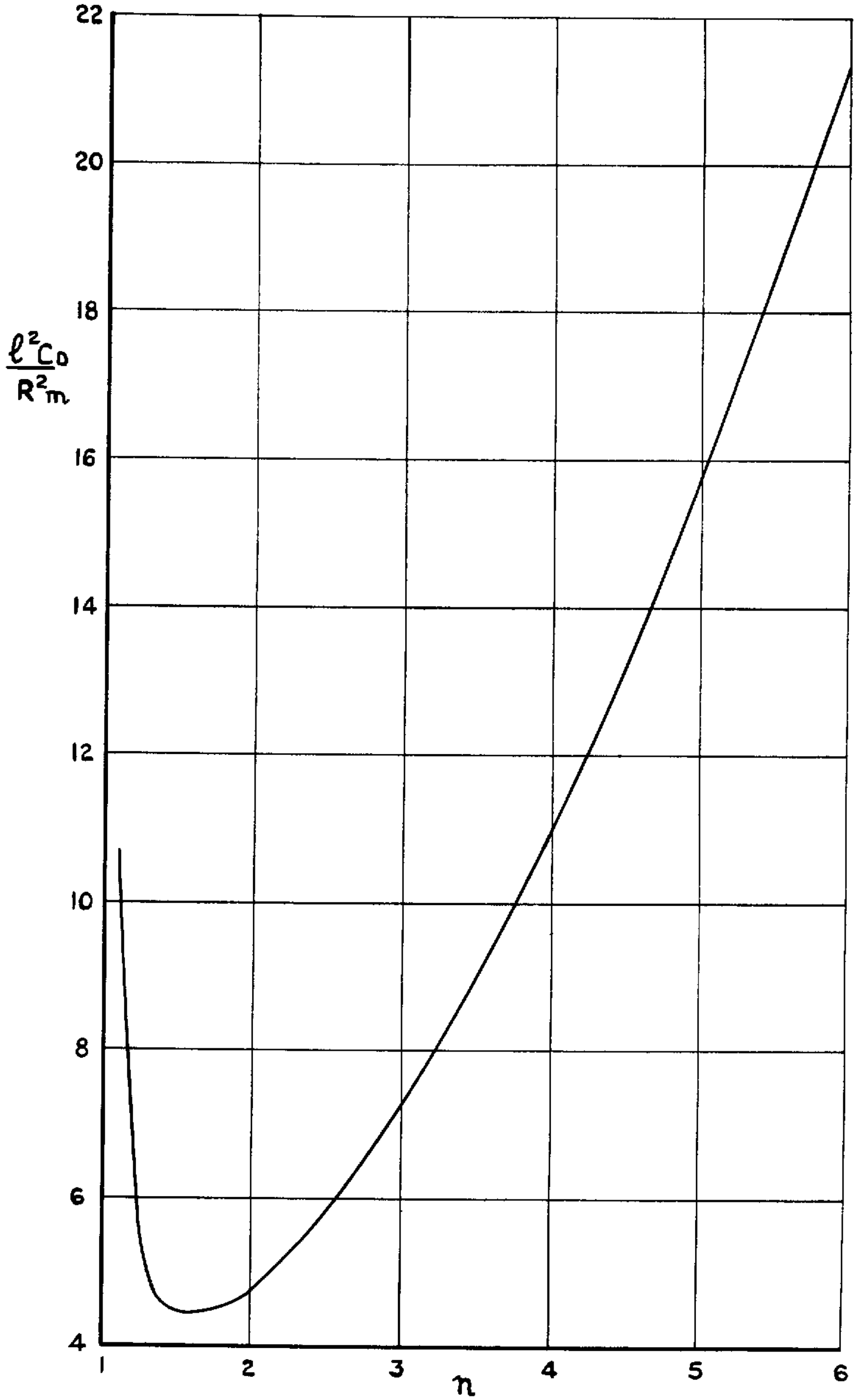

FIG. 5 (a) DRAG AS A FUNCTION OF n WITH $\frac{S_o}{S_m} = 0$ (POINTED NOSES)

FIG. 5(b).

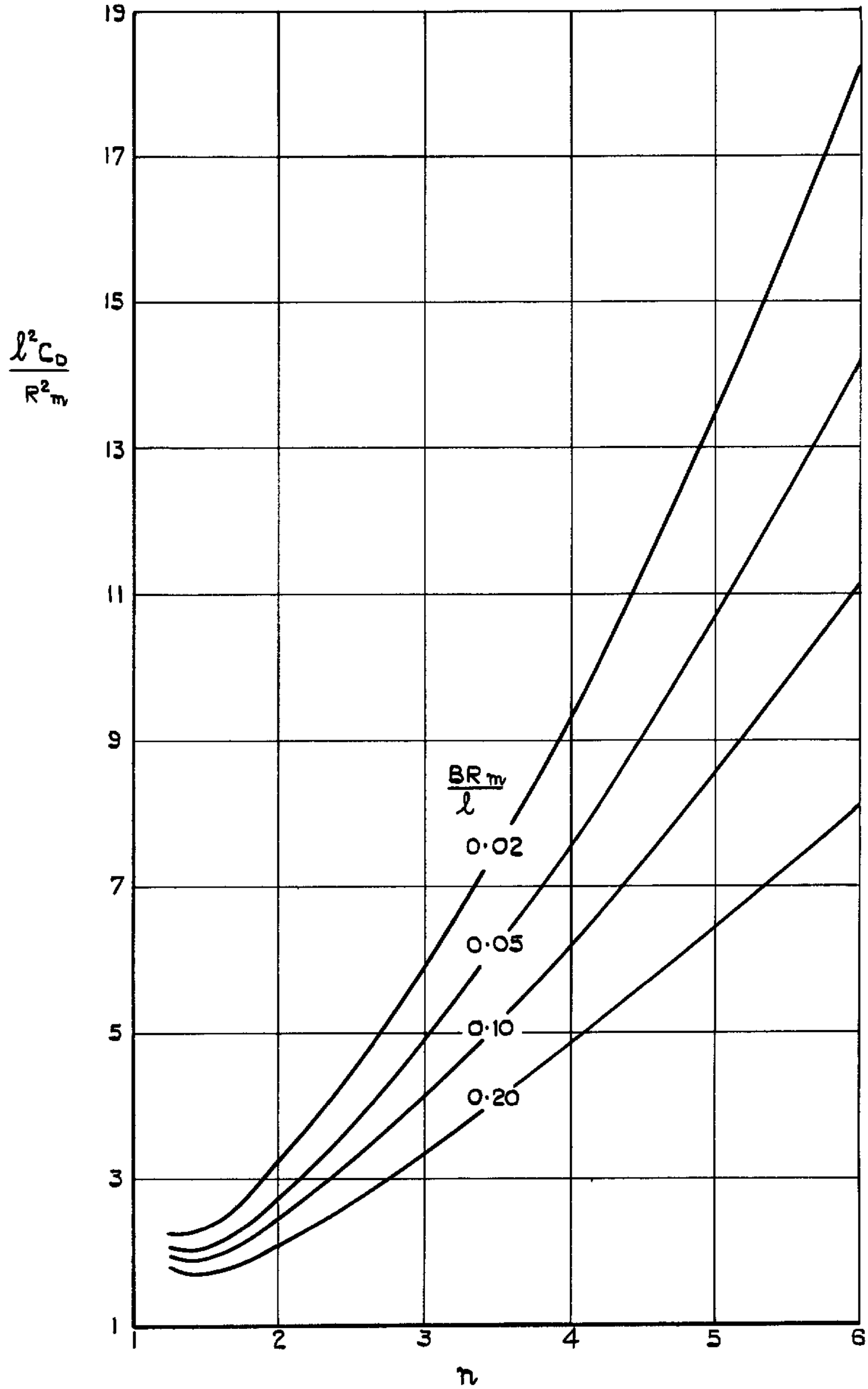

FIG. 5(b) DRAG AS A FUNCTION OF n WITH $\frac{S_0}{S_m} = 0 \cdot 3$.

FIG. 5(c).

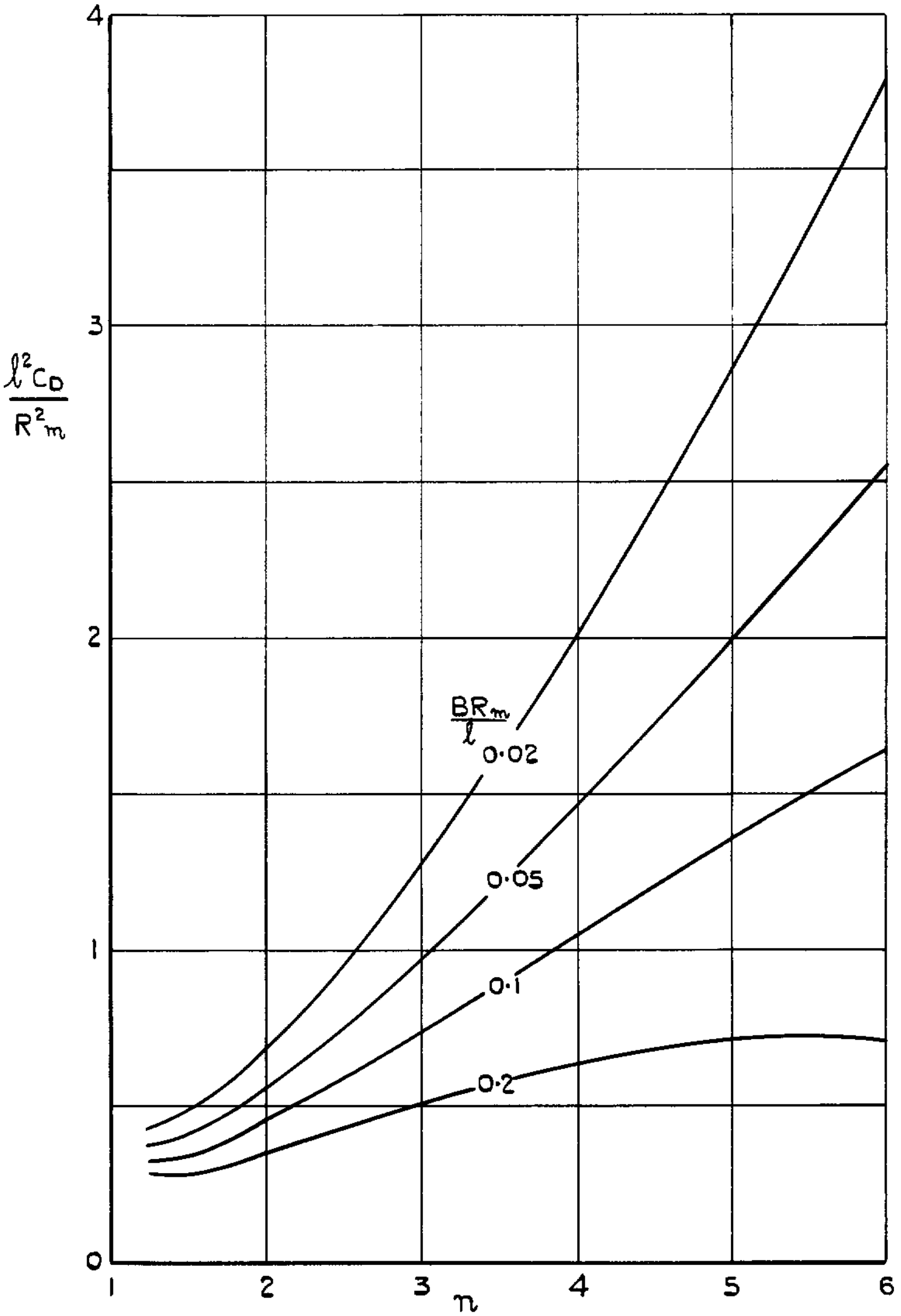

FIG. 5 (c) DRAG AS A FUNCTION OF n WITH $\frac{S_0}{S_m} = 0{\cdot}7$.

C.P. No. 245
(17,694)
A.R.C. Technical Report

Published by
HER MAJESTY'S STATIONERY OFFICE

To be purchased from
York House, Kingsway, London W.C.2
423 Oxford Street, London W.1
P.O. Box 569, London S.E.1
13A Castle Street, Edinburgh 2
109 St. Mary Street, Cardiff
39 King Street, Manchester 2
Tower Lane, Bristol 1
2 Edmund Street, Birmingham 3
80 Chichester Street, Belfast
or through any bookseller

PRINTED IN GREAT BRITAIN

S.O. Code No. 23-9009-45

Wt.2078.K3

C.P. No. 245